

December 17, 2024

NAC TR 24237-1

A Practical Guide to Tuning Spiking Neuronal Dynamics

Version 1

William Gebhardt*, **Alexander G. Ororbia II***, **Nathan McDonald**,
Clare Thiem, **Jack Lombardi**
The Neural Adaptive Computing Laboratory
Air Force Research Laboratory

A Practical Guide to Tuning Spiking Neuronal Dynamics

Version 1

William Gebhardt*, **Alexander G. Ororbia II***, **Nathan McDonald,**
Clare Theim, Jack Lombardi

The Neural Adaptive Computing Laboratory
Department of Computer Science, Rochester Institute of Technology

Contents

1	Introduction	3
2	Spiking Neuronal Building Blocks	3
2.1	Input Encoding Units	4
2.1.1	Bernoulli Encoding	4
2.1.2	Poisson Process Encoders	5
2.1.3	Phasor Encoders	5
2.1.4	Latency Encoders	6
2.2	Spiking Neural Units	7
3	Hyper-parameter Effects on Dynamics	11
3.1	Leaky Integrate-and-Fire Dynamics and Behavior	11
3.2	Excitatory and Inhibitory Neurons	13
3.2.1	Effects of Equally-sized Populations of Inhibitory and Excitatory Neurons	14
3.2.1.1	One-to-One, One-to-Many	14
3.2.1.2	One-to-Many, One-to-One	14
3.2.2	The 80-20 split	16
4	Conclusions and Outlook	16

*Authors contributed equally.

The views and conclusions contained herein are those of the authors and should not be interpreted as necessarily representing the official policies or endorsements, whether expressed or implied, of the Air Force Research Laboratory (AFRL) or the U.S. Government. This material has been cleared for public release, unlimited distribution. (PA Case #: AFRL-2025-1948).

1 Introduction

There are countless papers, efforts, and methods that utilize spiking neural networks (SNNs) to solve various modeling problems [10, 13, 12, 18, 9, 15]. Each of these efforts generally use their own specific formulation of SNN learning and topology to achieve their success in their research goals. Nevertheless, many of these SNN-centric efforts use foundational components and concepts – such as the basic neuronal cell building block or means of data encoding – that are generally shared at least partially across the different efforts. As these basic ingredients are found all over computational neuroscience and brain-inspired computing [20, 23], the knowledge of the hyper-parameters used, how to tune them, as well as the overall dynamical changes caused by alterations made to these hyper-parameter values has to regularly be gleaned in small doses from dozens of papers. In this work, we move to provide an overview of these common components and create a useful perspective on configuring and tuning these parameters. In addition, this empirical effort will provide examples of “collapsed” dynamical SNN systems, which are SNN models that exhibit behavior that is not necessarily wrong (mathematically) but are missing favorable properties of dynamics that might be expected in such computational systems.

This work will study¹ different key methods commonly used to encode real-valued data values into a format that is usable by SNNs, including both probabilistic and periodic methods, i.e., Bernoulli trials, Poisson processes, and phasors. We will further break down the formulation of two neuronal models: the leaky integrate-and-fire (LIF) neuron and the resonate-and-fire (RAF) neuron. Furthermore, we will examine how certain hyper-parameters affect LIF dynamics and then examine a small excitatory-inhibitory assembly of both LIF and RAF units, allowing us to study a basic SNN that embodies many of the key the dynamics that a modeler might come to expect.

Motivation: We write this article to serve as a teaching tool rather than an effort to fill a particular technical gap in brain-inspired computing or computational neuroscience. In other words, our contribution is the development of a much-needed practical guide for newcomer researchers and practitioners who need to build well-working SNN systems themselves. Our motivation in writing this article is twofold: **1)** we seek to provide a central piece that lays out how to tune certain components in SNNs, and **2)** our goal is to enable those who are new to SNNs in building their first biophysical models without having to dissect large bodies of literature in order to gather all of the requisite practical information. Note that this work will not be covering how to train a network, e.g., via Hebbian learning, or dealing with the dynamics of an evolving system [19]; instead, we will focus on setting up the dynamics for a randomly initialized network. Our rationale for ensuring that a non-evolved SNN is properly working is that, if the initial system is not functioning in an expected manner (“healthy” behavior), then it would be unreasonable to expect that an evolved system will reflect the expected behavior as well (possibly yielding further degenerate behavior).

2 Spiking Neuronal Building Blocks

A key first step in setting up a spiking neuronal system is to consider how the data input values and, in some cases, the output target values, e.g., labels, used to train output units of a spiking model, are to be represented. In the context of biophysical models that would further be suited for implementation on neuromorphic hardware, it is often important to design a scheme, at least for simulation, that effectively and efficiently encodes typically real-valued, continuous data features in terms of discrete

¹A supplement containing additional results/details can be found at: <https://github.com/NACLab/SnnDynamicsPracticalGuide>

spike pulses. This is motivated by the fact that the sensors typically coupled to neuromorphic systems, e.g., implemented spiking neural network (SNNs), will produce discrete, pulse-like values across time. In this section, we will study several key methods that one might employ in order to simulate discrete, temporal representations of (input) data that would be processed by SNN circuit models.

2.1 Input Encoding Units

Encoding a real-valued input into a spike train that is suitable for processing in an SNN can be done in a variety of ways. Many methods involve probabilistic or periodic sampling based on the intensity of the (sensory) input pattern. Inputs are usually normalized between zero and one, with zero representing the case of the encoding being ‘blank’ and one representing the largest frequency of events. Traditionally, whether or not the encoding is produced periodically or probabilistically, there is an overarching goal for the number of events present in an encoding to follow a Poisson distribution. This is further motivated by a range of experimental support in neurobiological studies [2] (the study in [2] found that, in the visual area MT, about one third of the cells studied exhibited spiking patterns compatible with Poisson processes).

Mathematically, a Poisson distribution can be thought of as the probability of k events happening in a given window of time, conditioned on the expected number of events λ (in the same window). In this section, we discuss some of the common methods for producing these different Poisson-distributed encodings and show how close they are at producing the desired number of events at different expected frequencies. For all following subsections, let f_e be the expected frequency of events over the duration of one second and let \hat{f}_e be the expected number of events per time step calculated as follows:

$$\hat{f}_e = f_e * \frac{\Delta t}{1000} \quad (1)$$

where Δt is in milliseconds per event, i.e., the integration time constant used later for the spiking neuron models.

2.1.1 Bernoulli Encoding

Encoding a real-valued number into a spike train using a Bernoulli distribution is perhaps the most straightforward and simplest method. At its core, a Bernoulli trial centers around the idea of flipping a weighted coin and counting the number of successful flips. If we treat each time step as its own independent flip of this coin, we get a sequence of Bernoulli trials which is referred to as a Binomial distribution. This distribution can be formally written terms of the probability of exactly k successes out of n trials as:

$$P(x) = \binom{n}{k} x^k (1-x)^{n-k}. \quad (2)$$

Since the above equation is expressed over n trials (or time steps) in the context of our model, this means that, in order to use it to produce a spike train, we will need to work with a precomputed spike train in order to properly sample the Binomial distribution. However, this can prove to be problematic since, normally, the goal is to work with an input encoder that can generate an encoding in synchronization with the data stream, often referred to as “encoding online” (or real-time encoding). In order to circumvent this limitation, we can instead set the number of successes (k) and trials (n) in the Binomial distribution to one. As a result, using these values, the equation for the probability mass

function collapses to:

$$P(x) = \binom{1}{1} x^1 (1-x)^0 = x. \quad (3)$$

Thus, we can see that constructing an online binomial distribution (or a Bernoulli trial) for encoding input data collapses to a single weighted coin flip conditioned on the normalized real value input, resulting in a fast sampling process.

2.1.2 Poisson Process Encoders

One common problem found in using a Bernoulli encoder is that, if the normalized input is one ($x = 1$), the Bernoulli encoder will produce a spike at every time step. This is, however, not an ideal scenario. SNNs rely on the temporal dynamics of the encoded spike trains and if spikes are emitted at every time step, then these temporal dynamics are lost or overshadowed (and time, in the case of independent Bernoulli trials, means very little, resulting in impoverished data encoding dynamics). Therefore, there is an extra transformation often applied to the input that produces a sparser output encoding; this transformation is as follows:

$$\hat{x} = x \hat{f}_e \quad (4)$$

where we observe that the above equation entails scaling the intensity probability of x by the expected number of events per time step. The above scaling results in a Poisson process, producing \hat{x} which is the transformed probability of emitting an event where the units are events per time step. This transformed value, when used in Equation 3, will produce an expected number of events that is scaled based on the normalized input value. This means, when expanded, the probability takes on the following form:

$$P(x; \Delta t, f_e) = x * f_e * \frac{\Delta t}{1000} = x * \hat{f}_e = \hat{x}. \quad (5)$$

However, while the above is a reasonable starting-point for encoding data into spike trains, there is a limitation to the use of a Poisson process encoding – the produced spike train will exhibit a high variance between the difference of spike timings. This is due to the fact that each event in the encoded spike(s) is independent of all the other events which results in a large variance in the time between events.

2.1.3 Phasor Encoders

If the neuronal structure requires a more regular spike pattern yet there is still a desire for the number of events to follow a Poisson distribution, then ‘phasor encodings’ can be used instead. A phasor represents a point moving around a circle at a fixed angular velocity, producing a sinusoidal wave. These encoders produce a spike every complete rotation that the point moves around the circle.

To start using a phasor to encode a continuous value, one must start by sampling a Poisson distribution with the expected number events that is equal to f_e . This sampled value is then set to be the actual firing rate of the phasor as follows:

$$f_n \sim P(\lambda = f_e). \quad (6)$$

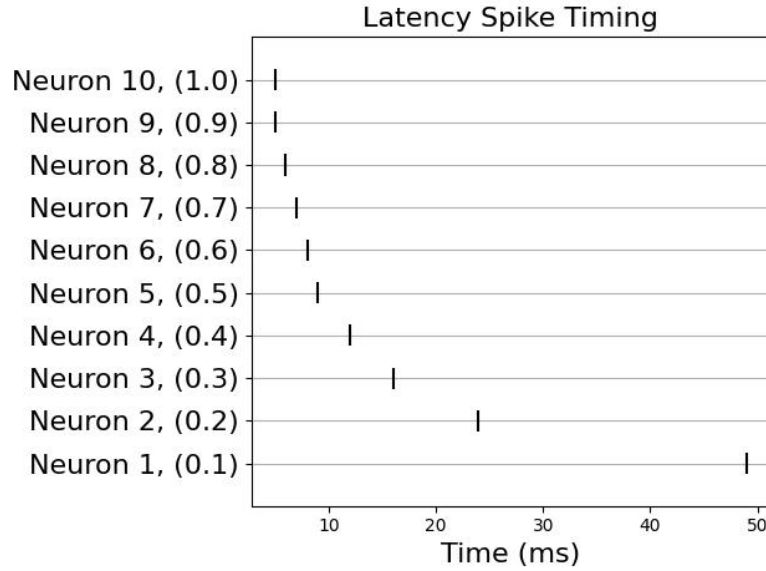


Figure 1: A latency-encoding spike train; probability values for ten input neurons were incrementally generated (through steps of 0.1) within the range [0.1, 1.].

As the number of neurons in the layer increase, their individual expected firing rates will converge to be a Poisson distribution. Using each phasor’s actual firing rate, the phasor’s angular velocity can then be calculated in the following manner:

$$v_n = 2\pi f_n = 2\pi * \frac{\Delta t}{1000} * f_n = \frac{\pi \Delta t}{500} * f_n. \tag{7}$$

The final units of v_n would then be in radians (rad) per time step. This means that, at every time step, the angle of the phasor can be updated by adding v_n to the current angle θ_n . To compute if a spike is produced over any particular time step, it is detected if the current angle θ_n is larger than 2π – an angle greater than this values results in a spike emission and a value of 2π is subtracted from the phasor’s angle. This process can be expressed in terms of the following functions:

$$\theta_n = \begin{cases} \theta_n & \theta_n < 2\pi \\ \theta_n - 2\pi & \theta_n \geq 2\pi. \end{cases} \tag{8}$$

Another trick that is performed to augment these phasor-based encodings is the injection of noise into the velocity at any given time step. This is done by sampling a normal distribution around 1 (with small variance) and adding this to the velocity. This allows for the inter-spike time between spikes emitted by the phasor to not be a constant and yet behave regularly enough such that the overall firing rate is not adversely affected.

2.1.4 Latency Encoders

Beyond encodings that follow a Poisson distribution to model the number of expected events from a given value, there is form of spike train generation known as the latency encoding. These encoders work by having the input values that are closer to the maximum input value emit spikes earlier than the input values that are closer to the minimum input value. In addition, each input neuron can only

emit one spike per time window; this means that there are significantly fewer events encoded by a latency cell when compared to the Bernoulli or the phasor encoding cells.

Latency encoding [5, 17] of continuous inputs is performed by treating sensory values as electrical current i_{in} that is injected into a resistor-capacitor (RC) circuit, like so:

$$v(t) = i_{\text{in}}R \left(1 - e^{-\frac{t}{RC}}\right) \quad (9)$$

where R is the input resistance scaling factor and C is the capacitance constant. When the circuit's input voltage value exceeds a threshold v_{thr} , a spike is emitted. In essence, this simplified RC circuit models means that, as the input grows larger in magnitude, the faster it will charge up the voltage $v(t)$ to its threshold (resulting in the emission of a discrete spike pulse). However, to produce the actual spike based on sensory input intensity, we solve Equation 9 for time t as follows:

$$t = \tau_{\text{in}} \ln \left(\frac{i_{\text{in}}}{i_{\text{in}} - v_{\text{thr}}} \right) \quad (10)$$

where $\tau_{\text{in}} = RC$ (R is, for convenience, usually set to one, allowing the experimenter to focus on setting the capacitance and τ values explicitly). Given the computed spike time t , we may produce a binary spike train encoding by create a T -length vector of zeros and setting the value at index t to one. In Figure 1, we show a controlled latency-coded spike train.

As a result of the above formulation, the input values are treated as a form of constant electrical current that is injected into the RC circuit. Note that a higher value of τ_{in} will induce a slower firing rate and has the effect of spreading out the spike times across the stimulus window time T . Generally, with a pre-defined v_{thr} , all input values below this threshold do not result in a close-form solution (given that the input current is not high enough to drive the membrane voltage $v(t)$ past its threshold) – in implementation, any value below this threshold is clipped and either assigned to the final time-step or removed entirely.

2.2 Spiking Neural Units

The Leaky Integrate-and-Fire Model: A model of neuronal dynamics that we seek to study is the leaky integrator, also known as the leaky integrate-and-fire [4, 14] (LIF) neuron. Historically, the equations that characteristically described the LIF were first proposed by Stein [22] in 1965. Since their conception, the dynamics for an LIF's voltage (v_k^ℓ) have been distilled to the following ordinary differential equation (ODE):

$$\tau_v \frac{\partial v_k^\ell(t)}{\partial t} = -\gamma_v (v_k^\ell(t) - v_{\text{rest}}) + R^\ell j_k^\ell(t) \quad (11)$$

where τ_v is the membrane potential time constant, γ_v is the voltage leak coefficient, v_{rest} is the membrane resting potential, and R^ℓ is the membrane resistance. Note that $j(t)$ is considered constant for the ODE above over ∂t .

The current that enters the LIF cell, $j_k^\ell(t)$, also evolves according to its own dynamics as dictated by the ODE below:

$$\tau_j \frac{\partial j_k^\ell(t)}{\partial t} = -\gamma_j j_k^\ell(t) + \kappa^\ell i_k^\ell(t) \quad (12)$$

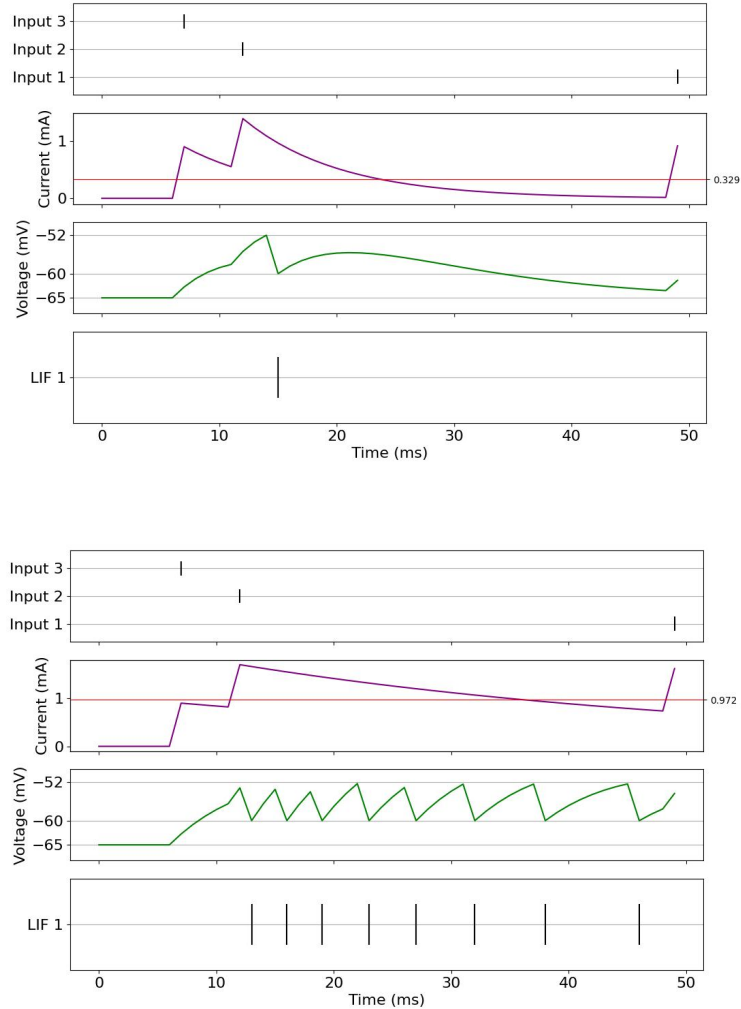


Figure 2: Latency-LIF coupled dynamics. Above is a visual of the dynamics of a four-cell system – 3 latency-coding input cells synaptically wired into 1 LIF cell – under two different time constant settings (left shows a “healthy” setting; right shows a “degenerate” setting). Both cases show the scenario where two initial latency-coded spikes occur near one another with the last one lagging behind. Notice, in the “healthy” setting, the closeness of two input spike pulses results in an output spike emission; the “degenerate” setting results in an unexpected, constant stream of output spikes emitted from just two input pulses.

where γ_j is the electrical current leak coefficient. Note that $i(t)$ is considered constant for the ODE above over ∂t . $i_k^\ell(t)$ itself could be directly-injected electrical current or the sum of weight values for non-zero pre-synaptic emission as follows:

$$i_k^\ell(t) = \sum_i \begin{cases} W_{ik}^\ell & s_i^{\ell-1} = 1 \\ 0 & \text{otherwise.} \end{cases} \quad (13)$$

where $s_i^{\ell-1}$ is a binary value denoting if there is a spike emission from pre-synaptic neuron i . The

equation governing the spike emissions (s_k^ℓ) for a given LIF neuron k is as follows

$$s_k^\ell(t) = \begin{cases} 1 & v_k^\ell(t) > \theta_k^\ell(t) \\ 0 & \text{otherwise} \end{cases} \quad (14)$$

where $\theta_k^\ell(t)$ is the membrane voltage threshold (which, once breached, results in the neuron emitting a discrete spike pulse). Furthermore, once a neuron k has emitted a pulse, it is hyper-polarized to a reset target voltage value v_{reset} :

$$v_k^\ell(t + \Delta t) \leftarrow v_k^\ell(t + \Delta t)(1 - s_k^\ell(t)) + v_{\text{reset}}s_k^\ell(t). \quad (15)$$

The voltage threshold is further made to be a function of time t and constructed to adhere to its own dynamics; this results in an ‘adaptive threshold’. Concretely, the threshold is a combination of a time-varying homeostatic (shift) variable $\hat{\theta}_k^\ell(t)$ and a fixed base threshold value $\theta_{\text{base}}^\ell$ yielding:

$$\frac{\partial \hat{\theta}_k^\ell(t)}{\partial t} = -\frac{1}{\tau_\theta} \hat{\theta}_k^\ell(t) + \kappa_\theta s_k^\ell(t), \quad \theta_k^\ell(t) = \theta_{\text{base}}^\ell + \hat{\theta}_k^\ell(t) \quad (16)$$

where τ_θ is the homeostatic variable time constant and κ_θ is the variable increment value. In Figure 2, we perform a small experiment examining the resulting dynamics of an LIF cell that is driven by a triplet of input latency-coding cells.

The Resonate-and-Fire Model: An important alternative model to the LIF is the resonate-and-fire (RAF) neuron [11] (also referred to as “resonator neurons”). Unlike LIFs, which integrate their input stimuli and prefer higher-frequency inputs in order to fire sooner (shorter distance between input pulses results in a higher likelihood of an LIF firing), RAFs are driven by the timing of pulses with relative to their period of oscillation. In other words, if two incoming pulses are near half the period, the input spikes will cancel each other out (and not result in the RAF firing) whereas, if their timing is near one period of oscillation, the spike pulses will add up (and result in the RAF emitting a pulse of its own). For any RAF to fire/spike, it will require stimulation at its resonant frequency (of its subthreshold oscillation). Unlike an LIF, an increase in the frequency of incoming spikes to an RAF might result in a delay of (even terminate) its own firing.

The RAF neuron can be constructed as a two-variable system for spiking cell dynamics, i.e., two coupled ODEs describe the RAF’s behavior. The RAF neuron specifically produces a trajectory that can be broken apart into a voltage state $v_k^\ell(t)$ (referred to as a “voltage-like variable” in [11]) and an angular driving state $c_k^\ell(t)$ (referred to as a “current-like variable” [11]). Formally, the RAF’s angular driving variable $c_k^\ell(t)$ adheres to the following dynamics:

$$\tau_c \frac{\partial c_k^\ell(t)}{\partial t} = c_k^\ell(t) * b - v_k^\ell(t) * \omega + R j_k^\ell(t) \quad (17)$$

where $j_k^\ell(t) = (\tau_v / \Delta t) * i_k^\ell(t)$ is the externally-injected input electrical current (scaled by resistance R) that flows into the RAF at time t ; ω is the (angular) eigenfrequency hyper-parameter (in Hertz) and b is the oscillation dampening factor. τ_c is the angular variable’s time constant in milliseconds (ms). The

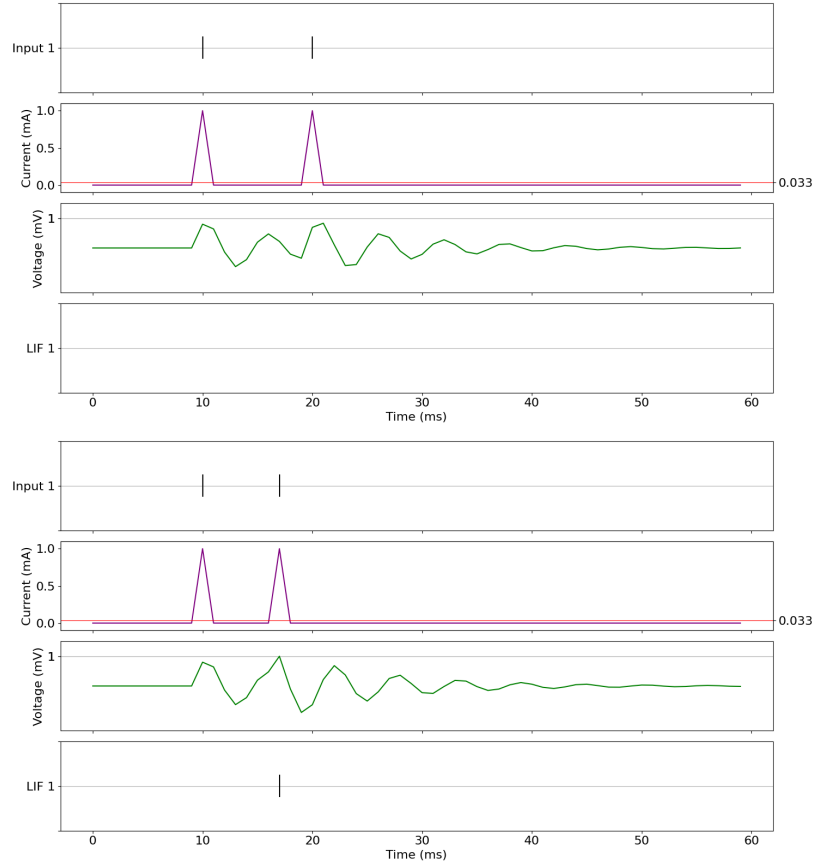


Figure 3: Resonate-and-Fire dynamics. Here, we visualize the dynamics of a resonate-and-fire (RAF) neuron under two important conditions: 1) a pair of input spikes, also known as a spike doublet, that are *not* resonant with the RAF unit (the interspike interval between the two pulses is not equal to the period of the RAF neuron, i.e., $T = 2\pi/\omega$) will not push the neuron beyond its threshold, and 2) a doublet that is resonant with the RAF unit will push it to emit a post-synaptic spike.

neuronal component $c_k^\ell(t)$ then drives the membrane potential (voltage) $v_k^\ell(t)$ which itself adheres to:

$$\tau_v \frac{\partial v_k^\ell(t)}{\partial t} = \omega * c_k^\ell(t) + v_k^\ell(t) * b \tag{18}$$

where, as in the LIF, τ_v is the membrane potential time constant (ms). To emit a spike/pulse, the RAF's voltage variable $v_k^\ell(t)$ is compared to a threshold value as in Equation 14 (as in the LIF), i.e., $s_k^\ell = 1$ if $v_k^\ell(t) > \theta_k^\ell(t)$; if the RAF unit spikes, its membrane voltage $v_k^\ell(t)$ and angular driving variable $c_k^\ell(t)$ can be set to their base/reset values, i.e., $v_k^\ell(t) = v_{\text{reset}}$ and $c_k^\ell(t) = c_{\text{reset}}$.

The RAF is, in effect, a coupled damped oscillator that is able to describe the subthreshold behavior of a spiking cell. Notably, when a dormant RAF cell is triggered by an excitatory input pulse, the unit will exhibit dampened oscillatory behavior (in accordance with the RAF's eigenperiod of $T_p = 2\pi/\omega$); as the neuron oscillates, there are certain windows of opportunity for the RAF unit to fire: **1**) if another pulse happens immediately after the first pulse (coincident detection), or **2**) if the second pulse happens one eigenperiod T_p away from the first (resonance detection). (Note that a second input spike will have the least effect when it is $T_p/2$ units away from the first spike.) Furthermore, an inhibitory spike would enhance the RAF unit's sensitivity to later excitatory pulses (that have the right timing) [11].

In Figure 3, we run a small simulation to examine the resulting dynamics of an RAF cell driven by a spike doublet (i.e., two input spikes spaced out in time) under two conditions to highlight its resulting output spike behavior: 1) a case where the spike doublet is not resonant with the RAF’s eigenfrequency, and 2) where the spike doublet is resonant with the RAF’s eigenfrequency.

3 Hyper-parameter Effects on Dynamics

3.1 Leaky Integrate-and-Fire Dynamics and Behavior

Here, we will examine effects that the membrane time constant, decay, and input coefficients have on LIF dynamics.

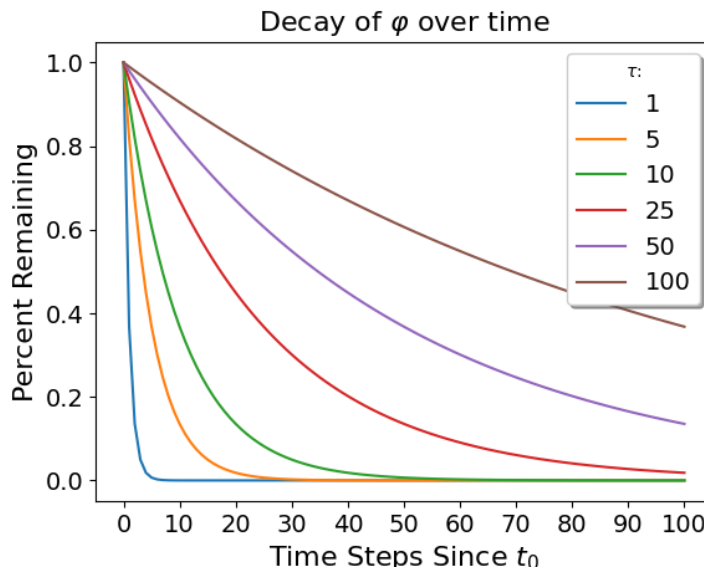


Figure 4: Comparison of different time constants (τ) and their effect on decay rate for exponentially decaying values.

The Membrane Time Constant: To gather an intuition behind membrane time constants – and time constants in general – in relation to the ODEs commonly found in computational neuroscience, we will first look at a general equation using abstract terms. If there is a value (φ) that exponentially decays with time (t), the dynamics of that decay can be adjusted with time constant τ . Starting with the equation:

$$\tau_{\varphi} \frac{\partial \varphi(t)}{\partial t} = -\varphi(t) \tag{19}$$

we can solve for the value exact value of φ , given the current time and the value at some t_0 . This results

in the following:

$$\begin{aligned}
 \tau_\varphi \frac{\partial \varphi(t)}{\partial t} &= -\varphi(t) \\
 \int \frac{1}{\varphi(t)} \partial \varphi(t) &= \frac{-1}{\tau_\varphi} \int \partial t \\
 \ln(\varphi(t)) &= \frac{-1}{\tau_\varphi} (t + C) \\
 \varphi(t) &= C e^{\frac{-t}{\tau_\varphi}} \\
 \varphi(t_0) &= C e^{\frac{-t_0}{\tau_\varphi}} \\
 C &= \varphi(t_0) e^{\frac{t_0}{\tau_\varphi}} \\
 \varphi(t) &= \varphi(t_0) e^{\frac{t_0 - t}{\tau_\varphi}} .
 \end{aligned} \tag{20}$$

This general equation for exponentially decaying values is used in a few places throughout the LIF; such as in the voltage and current ODEs. Note that the time constant is not the only coefficient governing the dynamics of these equations.

The Decay and Input Coefficients: In addition to the time constant τ_ν found in Equation 11, there are coefficients that scale both the decay rate (γ_ν) and the incoming input (R_ν). These two interact with τ_ν to either strengthen or weaken the effects of the time constant. Starting with:

$$\tau_\nu \frac{\partial \nu(t)}{\partial t} = -\gamma_\nu \nu(t) + R_\nu j(t) \tag{21}$$

we can say that if $\gamma_\nu = 1$ and $j(t) = 0$ for all t , then this equation functions identically to the one defined in (Equation 20). Now as γ_ν changes, its effects on τ_ν will be inversely proportional to the change. The effects of scaling τ_ν and the decay can be seen in (Figure 4). An alternative method for setting γ and τ_ν is to choose how many time steps a neuron should take before it is set to a specified proportion of the original value, given no extra input. As an example if a neuron is to reach 10% of the original voltage or

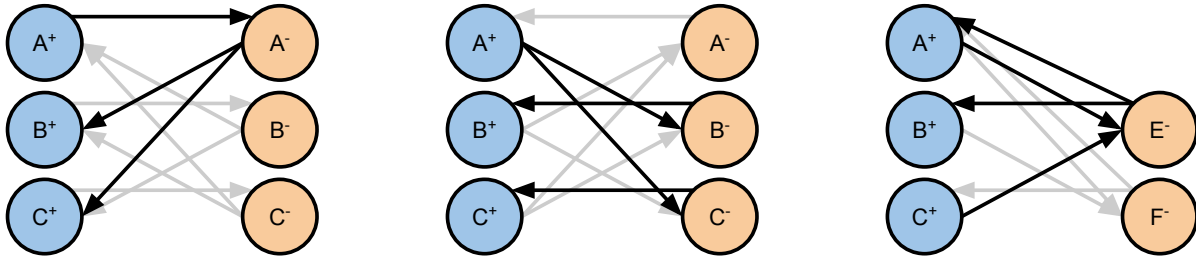


Figure 5: A visualization of various synaptic connectivity wiring patterns between a population of excitatory and inhibitory LIF cells: **(Left)** a one-to-one, one-to-many structure, **(Middle)** a one-to-many, one-to-one structure, and **(Right)** a sparsely-connected, random structure (with differently-sized populations, where there are fewer inhibitory neurons than excitatory ones).

0.1 $v(t_0)$ in a specific Δt , we can solve for the ratio via the following steps:

$$\begin{aligned} \tau_v \frac{\partial v(t)}{\partial t} &= -\gamma_v v(t) \\ v(t) &= v(t_0) e^{\frac{\gamma_v}{\tau_v}(t_0-t)} \\ v(t_0 + \Delta t) &= v(t_0) e^{\frac{\gamma_v}{\tau_v}(t_0-(t_0+\Delta t))} \\ 0.1 v(t_0) &= v(t_0) e^{\frac{-\gamma_v \Delta t}{\tau_v}} \\ 0.1 &= e^{\frac{-\gamma_v \Delta t}{\tau_v}} \\ \frac{-\ln(0.1)}{\Delta t} &\approx \frac{2.3}{\Delta t} = \frac{\gamma_v}{\tau_v}. \end{aligned}$$

In addition to scaling γ_v , the resistance value (R_v) in front of $j(t)$ can be used to control the impact that injected current supplied to the system has. Traditionally, R_v is scaled in terms of τ_v or ($R_v = \tau_v R'_v$) so that a consistent amount of current will be provided regardless of the system’s decaying dynamics.

3.2 Excitatory and Inhibitory Neurons

To create effective spiking neuronal network systems, one of the most important effects to usefully model is the balance of excitation and inhibition [24]. Excitatory and inhibitory pressures often entail a balancing act between signals that stimulate, or increase, the activity of neuronal cells and signals that depress, or decrease/dampen, the activity of neuronal cells. In this article, we conducted several experiments that study the ratio of excitatory-to-inhibitory neurons; concretely, we examine the biological ratio of 80%-20% (as known in the neocortex [16]) as well as equally-sized populations of both. Furthermore, we experiment with types of random synaptic connectivity that connect groups of excitatory and inhibitory neurons in our LIF-encoding and RAF-encoding SNN models.

3.2.1 Effects of Equally-sized Populations of Inhibitory and Excitatory Neurons

One of the common forms of inhibition is a fully-connected layer of excitatory neurons laterally wired to the same number of neurons in a separate inhibitory layer; this is a biophysical design pattern used in well-known models such as the SNN model of [8]. The matrix of cross-layer connections between these two layers of neurons (in either direction, i.e., excitatory-to-inhibitory and inhibitory-to-excitatory) normally takes on the form of either a hollow matrix (one-to-many) or of an identity matrix (one-to-one). The connectivity matrix between the layers will always consist of one of each of these types of matrices, with each setup having different implications on the dynamics that govern the paired excitatory-inhibitory groups.

3.2.1.1 One-to-One, One-to-Many Setting up an SNN model with a one-to-one set of connections from the excitatory neurons to the inhibitory neurons followed by a one-to-many set of connections from the inhibitory neurons to the excitatory neurons results in different effects depending on whether LIF or RAF neurons are used within the populations.

When using LIF neurons the effect that this inhibition pattern produces is similar to a winner-take-all (WTA) scheme, i.e., only one or a few neurons fire over a large period time. In practice, this effect is achieved through the quick firing of a few excitatory neurons which causes their corresponding inhibitory neurons to also fire quickly. This quick firing of a select group of inhibitory neurons dampens the stimulation of the other excitatory neurons. Since the initially spiking excitatory neurons will receive less of a dampening force (as compared to those that did not spike initially), they will, in turn, fire faster again, ultimately producing the WTA-like output. This result can be observed in Figure 6, specifically when comparing the model with no inhibition in Figure 6a to the model with inhibition in Figure 6c.

When tuning this particular structure, there are several factors to note: **1)** since there is significantly less stimulus being produced by the excitatory neurons, the resistance values (R) and the time constant (τ) of the inhibitory structure need to be increased relative to the excitatory structure in order to produce any spiking activity at all; **2)** adjusting the resistance of the excitatory-to-inhibitory connections will decrease the amount of excitatory activity needed to produce inhibitory activity; and, finally; **3)** adjusting the resistance of the inhibitory-to-excitatory connections increases the inhibiting effect of the structure and pushes it much closer to WTA behavior.

When using RAF neurons to build the neural populations, the effect that this inhibition pattern produces is akin to denoising. As RAF neurons require steady input of current to produce their spikes, when the inhibitory neurons end up firing, this can temporarily disrupt the firing of the excitatory neurons. If there is a constant enough disruption it can cause a neuron that had a long interspike timing to never fire; thus, this reduces the noise of random one-off spikes from the excitatory neurons. This result can be observed in Figure 6, specifically compared to the model with no inhibition in Figure 6b and the model with inhibition in Figure 6f.

3.2.1.2 One-to-Many, One-to-One The alternate way of setting up the models with an equal amount of excitatory and inhibitory neurons is with a one-to-many set of synaptic connections from the excitatory neurons to the inhibitory neurons and then a one-to-one set of connections from the inhibitory neurons to the excitatory neurons. As in the previous setup, there is a difference between the LIF and the RAF neurons; in fact, the resulting effects are swapped when as compared to the previous setup of one-to-one/one-to-many. The de-noising effect can be observed in the LIF neurons

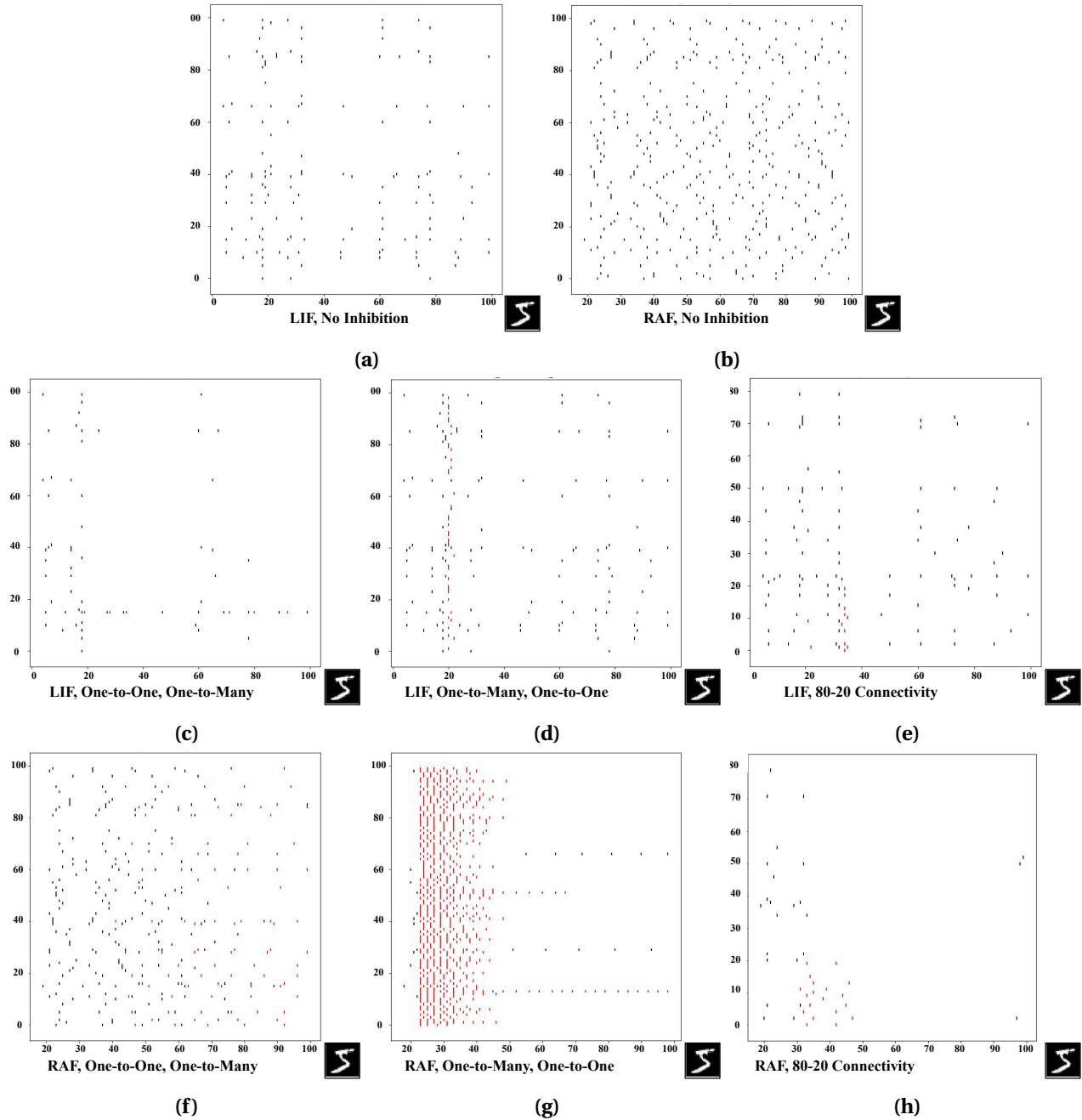


Figure 6: The effect that lateral synaptic connectivity – one-to-one/one-to-many, one-to-many/one-to-one, and sparse 80:20 split connectivity (with 80:20 ratio of excitatory-to-inhibitory units) – has on dynamics of two populations (one excitatory & one inhibitory) of LIFs and RAFs. In all plots, black ticks correspond to events in excitatory neurons; likewise, red ticks correspond to inhibitory neuron events. For the 80:20 split, there will only be red ticks from neuron index 0 to 20 (for inhibitory neurons).

by comparing Figure 6a and Figure 6d. Likewise, compare Figure 6b and Figure 6g to observe a WTA effect in the RAF neurons.

3.2.2 The 80-20 split

The construction of the ratio of 80% excitatory neurons to 20% inhibitory neurons was not chosen at random, but instead motivated by neurophysiological and computational studies of the proportion of excitatory to inhibitory neuronal cells in particular brain regions/structures such as the neocortex [16, 7, 1]²; it is notable that in an adult mouse brain, the excitatory-to-inhibitory ratio is approximately 8:2 [21]. Under this setup, there cannot be a one-to-one set of synapses connecting together the neurons of this pair of populations as the connection matrices are always densely connected with a roughly 20% dropout rate (i.e., about 20% of values are set to zero). The effects of this structure of neurons are also not mirrored in either of the two previous structures. Instead, an 80%-20% format effectively functions as a threshold applied to the total activity from excitatory neurons before inhibiting all of them; this effectively slows down or stops future neural activity. This dampening leads to an initial spike pattern found in the excitatory neurons to carry more weight as, after a short amount of time, the spiking decreases significantly. See Figures 6e and 6h for a raster plot depicting the result of our experimental study of the effect that an 8:2 ratio wiring pattern has on dynamics.

4 Conclusions and Outlook

In this work, we studied and experimentally analyzed practical elements to tuning various forms of input encoding for spiking neural networks, two fundamental building block neuronal cells – the leaky integrate-and-fire and the resonate-and-fire cell – used to construct spiking circuit models, and the effects of various design patterns for assemblies of leaky integrators and resonators, particularly in laterally-wired populations of excitatory and inhibitory neuronal cells. This empirical, simulation-based work is meant to provide a detailed starting point for researchers, engineers, and practitioners in brain-inspired computing and computational neuroscience who seek to construct their own biophysical neuronal models, particularly those that are building with spike-emitting / pulse-based computational units. An important future extension of this study should include an examination of the effect that spike-timing-dependent plasticity [3, 6] has on the neuronal dynamics of leaky integrators and resonators, once an SNN circuit has been set up according to the baseline prescriptions, hyper-parameter considerations, and lateral excitatory-inhibitory connectivity patterns studied in this work for a randomly initialized, static model configuration.

References

- [1] ALREJA, A., NEMENMAN, I., AND ROZELL, C. J. Constrained brain volume in an efficient coding model explains the fraction of excitatory and inhibitory neurons in sensory cortices. *PLOS Computational Biology* 18, 1 (2022), e1009642.
- [2] BAIR, W., KOCH, C., NEWSOME, W., AND BRITTEN, K. Power spectrum analysis of bursting cells in area mt in the behaving monkey. *Journal of Neuroscience* 14, 5 (1994), 2870–2892.
- [3] BI, G.-Q., AND POO, M.-M. Synaptic modifications in cultured hippocampal neurons: dependence on spike timing, synaptic strength, and postsynaptic cell type. *Journal of neuroscience* 18, 24 (1998), 10464–10472.

²The more general principle is that there are more excitatory neurons in relation to inhibitory ones where some ratios that have also been examined include 3:1 and 9:1 across animal species.

- [4] BURKITT, A. N. A review of the integrate-and-fire neuron model: I. homogeneous synaptic input. *Biological cybernetics* 95 (2006), 1–19.
- [5] CHASE, S. M., AND YOUNG, E. D. First-spike latency information in single neurons increases when referenced to population onset. *Proceedings of the National Academy of Sciences* 104, 12 (2007), 5175–5180.
- [6] DAN, Y., AND POO, M.-M. Spike timing-dependent plasticity of neural circuits. *Neuron* 44, 1 (2004), 23–30.
- [7] DECO, G., PONCE-ALVAREZ, A., HAGMANN, P., ROMANI, G. L., MANTINI, D., AND CORBETTA, M. How local excitation–inhibition ratio impacts the whole brain dynamics. *Journal of Neuroscience* 34, 23 (2014), 7886–7898.
- [8] DIEHL, P. U., AND COOK, M. Unsupervised learning of digit recognition using spike-timing-dependent plasticity. *Frontiers in computational neuroscience* 9 (2015), 99.
- [9] GEBHARDT, W., AND ORORBIA, A. G. Time-integrated spike-timing-dependent-plasticity. *arXiv preprint arXiv:2407.10028* (2024).
- [10] GERSTNER, W. Spiking neurons. *Pulsed neural networks* (1998), 3–53.
- [11] IZHIKEVICH, E. M. Resonate-and-fire neurons. *Neural networks* 14, 6-7 (2001), 883–894.
- [12] IZHIKEVICH, E. M. Polychronization: computation with spikes. *Neural computation* 18, 2 (2006), 245–282.
- [13] MAASS, W. Computing with spiking neurons. *Pulsed neural networks* 2 (1999), 55–85.
- [14] NAUD, R., AND GERSTNER, W. The performance (and limits) of simple neuron models: generalizations of the leaky integrate-and-fire model. In *Computational systems neurobiology*. Springer, 2012, pp. 163–192.
- [15] N’DRI, A. W., GEBHARDT, W., TEULIÈRE, C., ZELDENRUST, F., RAO, R. P., TRIESCH, J., AND ORORBIA, A. Predictive coding with spiking neural networks: a survey. *arXiv preprint arXiv:2409.05386* (2024).
- [16] NOBACK, C. R., RUGGIERO, D. A., STROMINGER, N. L., AND DEMAREST, R. J. *The human nervous system: structure and function*. Springer Science & Business Media, 2005.
- [17] OH, S., KWON, D., YEOM, G., KANG, W.-M., LEE, S., WOO, S. Y., KIM, J., AND LEE, J.-H. Neuron circuits for low-power spiking neural networks using time-to-first-spike encoding. *IEEE Access* 10 (2022), 24444–24455.
- [18] ORORBIA, A. Spiking neural predictive coding for continually learning from data streams. *Neuro-computing* 544 (2023), 126292.
- [19] ORORBIA, A. G. Brain-inspired machine intelligence: A survey of neurobiologically-plausible credit assignment. *arXiv preprint arXiv:2312.09257* (2023).

- [20] PARHI, K. K., AND UNNIKRISHNAN, N. K. Brain-inspired computing: Models and architectures. *IEEE Open Journal of Circuits and Systems 1* (2020), 185–204.
- [21] RODARIE, D., VERASZTÓ, C., ROUSSEL, Y., REIMANN, M., KELLER, D., RAMASWAMY, S., MARKRAM, H., AND GEWALTIG, M.-O. A method to estimate the cellular composition of the mouse brain from heterogeneous datasets. *PLOS Computational Biology 18*, 12 (2022), e1010739.
- [22] STEIN, R. B. A theoretical analysis of neuronal variability. *Biophysical journal 5*, 2 (1965), 173–194.
- [23] YAMAZAKI, K., VO-HO, V.-K., BULSARA, D., AND LE, N. Spiking neural networks and their applications: A review. *Brain sciences 12*, 7 (2022), 863.
- [24] ZHOU, S., AND YU, Y. Synaptic ei balance underlies efficient neural coding. *Frontiers in neuroscience 12* (2018), 46.